applied sciences

MDPI

Article

Group Pile Effect on Temperature Distributions inside Energy Storage Pile Foundations

Dilnura Sailauova [1], Zhamilya Mamesh [1], Dichuan Zhang [1,*], Deuckhang Lee [2,*], Chang-Seon Shon [1] and Jong R. Kim [1]

[1] Department of Civil and Environmental Engineering, School of Engineering and Digital Sciences, Nazarbayev University, Nur-Sultan 010000, Kazakhstan; dilnura.sailauova@nu.edu.kz (D.S.); zhamilya.mamesh@nu.edu.kz (Z.M.); chang.shon@nu.edu.kz (C.-S.S.); jong.kim@nu.edu.kz (J.R.K.)

[2] Department of Architectural Engineering, Chungbuk National University, Cheongju 28644, Korea

* Correspondence: dichuan.zhang@nu.edu.kz (D.Z.); dk@cbnu.ac.kr (D.L.)

Received: 19 August 2020; Accepted: 20 September 2020; Published: 21 September 2020

Abstract: Energy storage pile foundations are being developed for storing renewable energy by utilizing compressed air energy storage technology. Previous studies on isolated piles indicate that compressed air can result in pressure and temperature fluctuations in the pile, which can further affect safety of the pile foundation. Meanwhile, the temperature changes and distributions for the pile and surrounding soil also are influenced by adjacent piles in typical group pile constructions. Therefore, dynamic thermal transfer simulations were conducted in this paper to investigate the temperature changes and distributions in the concrete pile and surrounding soil for group pile construction. The main parameter in this study is the spacing of the piles. The analysis results show that the group pile effect significantly increases the temperature up to more than 100 °C depending on the location and changes its distribution in both concrete and soil due to the heat transferred from the adjacent piles. The final stabilized temperature can be as high as 120 °C in the concrete pile and 110 °C in the soil after numerous loading cycles, which is about 4 times higher than typical thermo-active energy pile applications. Thus, it is important to include the group pile effect for design and analysis of the energy storage pile foundation.

Keywords: group pile construction; thermal transfer simulation; energy storage pile; dynamic analysis

1. Introduction

A common method for utilizing renewable energy is to immediately generate electric power for operation of the building via solar panels that are directly attached to residential or commercial buildings [1]. This method eliminates energy loss due to long-distance transportation and maximizes power efficiency for usage. However, the energy generated by these alternative sources has an intermittent nature: they are dependent on climate and daily cycles [2]. Thus, an efficient storage for renewable energy is needed to accommodate the fluctuation of energy supply and to meet customer demand.

Reinforced concrete pile foundations have been proposed for renewable energy storage by utilizing compressed air energy storage (CAES) technology [3,4]. The pile foundation is designed with a hollow section, inside which renewable energy can be stored as compressed air and can be released to meet the customer demand. Since high pressure and temperature changes can originate from the compressed air during compressing and releasing processes, it can induce mechanical and thermal stresses, challenging the safety of the foundation. The structural responses of the foundation subjected to high pressure have been studied extensively [5,6]. The temperature distribution inside the pile foundation for isolated piles has also been investigated [7]. On top of these research results,

this paper presents a study on the temperature changes and distributions for the group pile construction since it is a common construction practice. Non-steady-state dynamic thermal transfer simulations were conducted for the group pile under cyclic temperature loadings generated by the compressed air. The magnitudes of the cyclic temperature loading were estimated based on the thermodynamic processes of the CAES. To carry out the heat transfer analysis, a two-dimensional (2D) plane strain model with concrete and soil layers was constructed. During the simulations, this model was subjected to fluctuating temperature inputs applied to the inner surface of the concrete pile. Pile spacing was considered a primary study parameter to evaluate the group pile effect on the temperature distribution inside the concrete section and the surrounding soil.

Similar thermal transfer analyses and temperature distribution studies were conducted extensively for thermo-active pile foundations [8–19]. In these studies, the pile was treated as a heat absorber for heat exchange between the ground surface and underground regions since the temperature at the ground surface fluctuates seasonally while the underground temperate remains constant. However, the thermal behavior for the energy storage pile discussed in this paper is different from that of the thermo-active pile foundation. These differences originated from the following:

(1) Different heat sources. The thermo-active pile is typically heated up or cooled down by the liquid circulating inside the pile, while the energy storage pile is subjected to temperature changes from the compressed air.
(2) Different locations of the thermal loading. The thermo-active pile is typically heated up or cooled down inside the pile section, while the energy storage pile is heated at the inner surface by the compressed air.
(3) Different magnitudes of the thermal loading. The thermo-active pile has a temperature change in the range of 10 to 20 °C for typical applications and can be as high as 30 °C for extreme heat exchanges [12]. On the other hand, the energy storage pile can result in a temperature increase up to more than 100 °C.

Because of these differences, it is not suitable to directly use the research results from the thermo-active pile foundations for the design of the energy storage foundation. Instead, the temperature changes and distributions from the thermo-active pile in current literature will be used as a reference to compare the results obtained in this paper.

2. Research Background

2.1. Thermodynamic Cycles

CAES technology is designed to use an advanced adiabatic cycle [20]. This cycle consists of 4 steps: compression, cooling, heating, and expansion (see Figure 1).

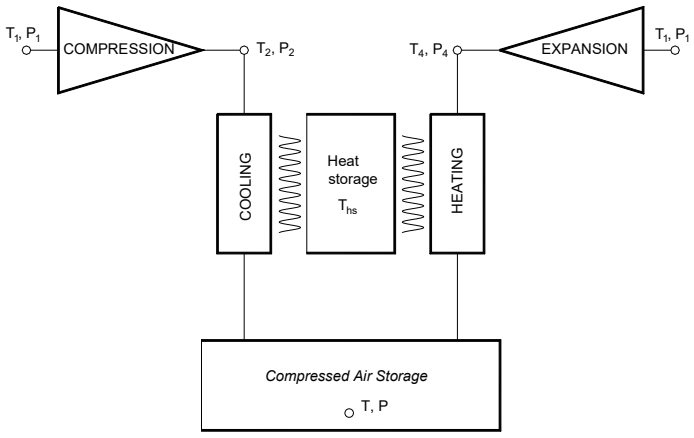

Figure 1. Thermodynamic processes of compressed air energy storage (CAES) (modified from [7]).

Firstly, the renewable energy generated from solar panels is used to compress the air with initial temperature (T_1). During this process, the compressor is activated by the power generated from the solar panels. As a result, the temperature and pressure of the air increase considerably, making it impossible to directly store the compressed air inside the concrete piles. After this stage, the temperature (T_2) of air can exceed 1000 °C. Thus, cooling is needed to reduce the temperature. In this step, the heat is extracted and placed inside another storage medium. This stored heat will then be used during release of the compressed air to heat it up before expansion. During the cooling stage, the efficiency of the cooling process prevents the temperature (T) from returning to the initial value (T_1). Although the storage temperature can be as high as 150 °C, it is still possible to be stored in the pile foundation since such a temperature has a negligible impact on the strength and stiffness of the concrete [21]. Next, as the power supply from the solar panels becomes unavailable, the energy stored as compressed air is released from the piles passing through the heating and expansion stages.

2.2. Group Pile Foundation

In typical deep foundations, a structural column is supported on a group of piles that are joined to a solid cap (see Figure 2). The behaviors of the single pile and the group pile are usually different due to the pile-to-soil interaction. Therefore, the term "group pile effect" is introduced to refer to the influence of piles on the behavior of nearby soils and piles. The group pile effect varies with the pile spacing (s) which is the center-to-center distance between adjacent piles. Several analytical and experimental studies were conducted to evaluate the mechanical behavior of the group pile and the pile–soil interaction [22–24]. In practice, the spacing is determined based on factors such as group pile efficiency, overlapping stresses, and cost of foundation [25]. Typically, it is recommended to use a minimum of 2.5 times the pile diameter as the pile spacing [26]. For the pile foundation proposed here, the group pile effect is expected to influence the temperature magnitude and distribution in both the pile section and the soil. As illustrated in Figure 2, each pile is first heated at the inner surface by compressed air (Figure 2a). Then, the heat starts to transfer outwards and gradually penetrates through the concrete section and soil (Figure 2b). After the heat penetration reaches the centerline between two piles (Figure 2c), the group pile effect starts to be activated and influences the temperature distribution of the soil and eventually the concrete pile on the other side (Figure 2d). Considering the hollowed pile geometry, this paper studies and quantifies the effect of group piles with 1-m outer diameter for pile spacing ranging from s = 2 m to 7 m.

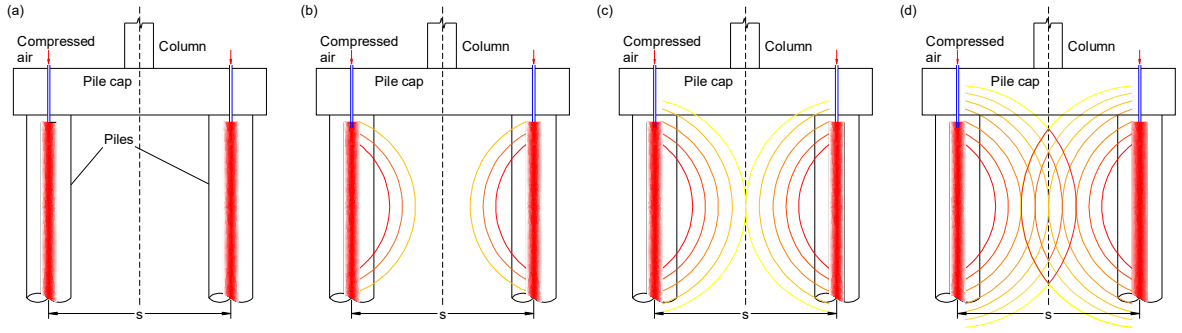

Figure 2. Thermal transfer in group piles for energy storage: (**a**) initial heating; (**b**) heat transferring; (**c**) heat reaching the center of piles; (**d**) heat penetrating to adjacent piles.

2.3. Performacne of Thermal-Active Energy Piles

Previous experimental and analytical studies on the thermo-active pile foundation have shown that the temperature changes and thermal-induced stresses in the soil are not critical under the operating conditions of typical applications [8–19]. However, the temperature changes in the soil may become significant under extreme thermal loading conditions (up to 30 °C) due to intensive uses of the energy piles [12,14,15,18]. The steady-state temperature in the soil for the group pile foundation is higher than

that for the isolated pile due to the thermal interactions between adjacent piles [12,15–19]. The more piles in a group, the higher the soil's temperature was observed [18,19]. Since the thermal transfer mechanism is similar between the thermo-active pile and the energy storage pile, comparisons of the temperature distributions between these two applications are conducted in this paper, although the loading conditions are quite different for these two cases.

3. Description of Thermal Loading and Models

3.1. Determination of Storage Temperature

Thermodynamic cycles of CAES can be used to calculate the temperature and pressure in the air stored inside the pile. The equations obtained from the energy balance principals and ideal gas equations can be expressed as follows:

$$\frac{V_s}{C^{7/2}}\left(\frac{T-\eta_2 T_1}{1-\eta_2}\right)^{5/2} = \frac{\dot{w}_{in}\eta_1 t_{in}}{3.5R} / \left(\frac{T-\eta_2 T_1}{1-\eta_2} - T_1\right) + \frac{\rho_i V_s}{\mu} \quad (1)$$

$$P = \frac{RT}{C^{7/2}}\left(\frac{T-\eta_2 T_1}{1-\eta_2}\right)^{5/2} \quad (2)$$

where the definitions and values of the parameters in Equations (1) and (2) are presented in Table 1. By solving the equations above with available storage energy ($\dot{w}_{in}$) and available volumes (V_s) for storage, the temperature and pressure demand for the pile can be determined. The derivation of Equations (1) and (2) was explained in detail in [6].

Table 1. Parameters in the thermodynamic equations.

Parameters	Definitions	Adopted values
R	Universal gas constant	8.31 J/(mol·K)
T_1	Ambient temperature	20 °C
C	Thermal constant	10.89
t_{in}	Compressing time	3600 s
ρ_i	The initial density of air	1.2 kg/m^3
μ	The molar mass of air	0.029
η_1	Efficiency of compression	75%
η_2	The efficiency of heat exchange and storage	90%

Using Equations (1) and (2), the storage pressure and temperature were calculated for different building geometries and design parameters. The detailed calculations were presented in [6] for different cases including numbers of building stories, different column spacings, and different inner diameters of the pile. From the calculations, a critical case was chosen, which has a 7-m column spacing, two stories, and a 200-mm pile inner diameter. This case produces the highest storage pressure and temperature, as show in Figure 3. As the column spacing increases, the stored energy for one single column will increase due to the increase in the tributary area. On the other hand, the larger column spacing will result in a longer pile length due to the higher tributary loading area, which can provide a larger available volume for energy storage. Therefore, the storage temperature and pressure are not sensitive to the change in column spacing. For a given column spacing, different pile group designs can be developed which permit the study of different pile spacings using the same temperature loading for the 7-m column spacing case.

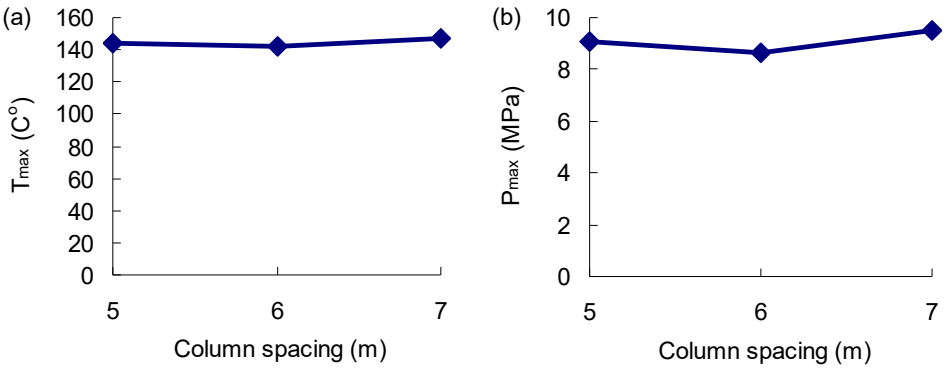

Figure 3. Maximum storage (**a**) temperature and (**b**) pressure vs. column spacing.

Figure 4 illustrates storage energy (Figure 4a), calculated storage temperature (Figure 4b), and storage pressure (Figure 4c) for a 24-hour cycle from 7:00 to 7:00 (next day) for the case of a 2-story building, 7 × 7 m column spacing, and 200-mm inner diameter (d_i). When the solar energy starts to be generated and the supply is higher than the demand, the available storage energy starts accumulating at 7:00 (see Figure 4a). When the solar energy becomes unavailable and the supply is less than the demand, the stored energy starts releasing at 19:00 (see Figure 4a). The temperature and pressure follow the energy storage and release cycle increase from 7:00, reaching maximum values at 19:00 (the middle of the cycle) when the storage energy starts to become unavailable. Then, temperature and pressure decrease to release the energy, returning to their original value at 7:00 of the next day. This temperature and pressure loading cycle might have lower values if the available storage energy reduces. However, for engineering design purposes, the temperature and pressure shown in Figure 4 is treated as the most critical case and is applied for the analyses presented in this paper.

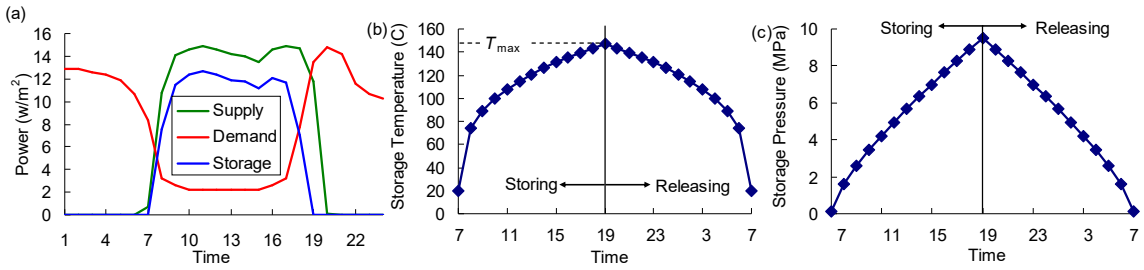

Figure 4. Daily energy storage cycle for 2-story, 7 × 7 m column spacing, d_i = 200 mm: (**a**) energy available for storage; (**b**) temperature; and (**c**) pressure.

3.2. Study Parameters

The main parameter considered in this paper is pile spacing (s), which is the center-to-center distance between two adjacent piles. Based on typical group pile foundation constructions discussed in Section 2.2, five spacing values ranging from 2 m to 7 m were selected for analysis of the group pile effect. In addition, an ideal isolated pile foundation case was considered as a reference case. This isolated pile was modeled with a soil layer of 41 m. At this distance, the soil temperature remains at the initial value and is not affected by thermal loading for the isolated pile case only [7]. The selected values of pile spacing for 6 different cases are s = 2 m, 4 m, 5 m, 6 m, 7 m, and the isolated pile case.

3.3. Analytical Model

A quarter of the pile and surrounding soil with a thickness equal to $s/2$ was cut out because of the symmetric plan of the group pile foundation, as shown in Figure 5a. Then, it is modeled as 2D plane strain elements in the general-purpose finite element software Abaqus FEA (see Figure 5b), one of

typical 2D simplifications used in structural simulations [27]. Symmetry boundary conditions were applied as there is no heat flux passing through the boundaries. The inner diameter (d_i) was selected as 200 mm. The thickness of the surrounding soil was calculated based on the pile spacing values discussed in the section above. The concrete section was divided into a mesh size of 10 by 20 mm with equal dimensions, whereas the soil layer has a gradually increasing size for the mesh along the radial direction.

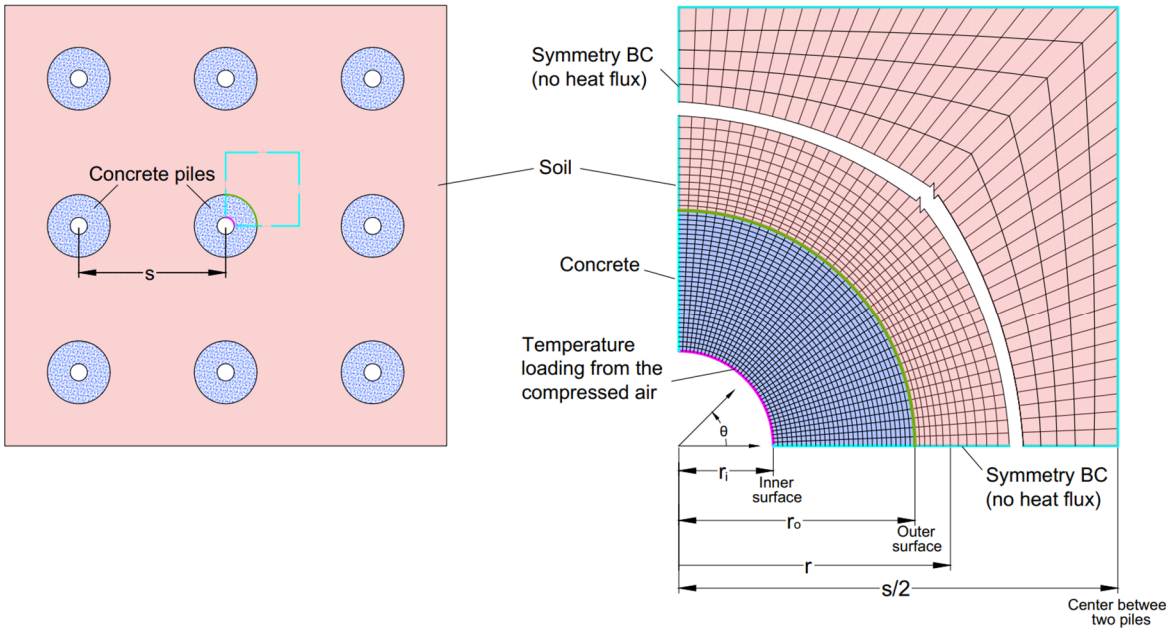

Figure 5. Analytical model of (**a**) group piles and (**b**) 2D plane strain model.

The dynamic thermal transfer simulation was carried out by imposing cyclic thermal loading at the interior surface of the concrete section. The backward Euler method with unconditional stability was used in the time integration procedure, which uses a backward difference algorithm (Equation (3)) to solve the basic energy balance equation (Equation (4)). The detailed solution algorithm and equations can be found in [28].

$$\dot{U}_{t+\Delta t} = (U_{t+\Delta t} - U_t)(1/\Delta t) \tag{3}$$

$$\int_V \rho \dot{U} dV = \int_V q dS + \int_V r dV \tag{4}$$

where V is the volume of the model; S is the surface area; ρ is the density of the material; $\dot{U}$ is the material time rate of the internal energy; q is the heat flux per unit area; and r is the heat supplied internally per unit volume. The integration time increment was automatically adjusted during the simulation to control the Courant–Friedrichs–Lewy value to be no more than 1.0. The concrete cracking effect on the thermal properties was ignored because the proposed new energy storage foundation uses high-performance concrete limiting the development of cracks [5,29]. The cyclic thermal loading follows the temperature change curve of a one-day cycle, as shown in Figure 4b. One thousand cycles of the thermal loading were conducted to ensure the convergence to a steady-state condition. The predefined initial temperature of the model was assigned as 12 °C, which resides within a range of normal underground temperatures (10 to 15 °C according to [30]).

The thermal properties of concrete were selected based on the results of the parametric study discussed in [7]. Since the energy storage pile requires high-strength concrete according to [5], this paper selected values of the thermal conductivity (2 W/m·°C) and specific heat capacity (940 J/kg·°C), respectively, which are suitable for high strength concrete [31,32].

The thermal conductivity for the soil was selected for mild moist (9%) fine sand at 1.0 W/m·°C, according to [33]. This value will typically reduce with the decrease in moisture content in the soil. For the energy storage pile, the moisture content in the soil is expected to decrease due to heating. The thermal conductivity of the soil will reduce as the temperature increases, which makes using a temperature-dependent nonlinear thermal material model necessary. However, considering that the number of cycles required to a reach steady-state is quite large (approximately 1000 cycles), a linear thermal material model with a fixed thermal conductivity was used to save computational cost. This simplification is deemed reasonable and provides a conservative temperature distribution for the engineering design purpose by ignoring the possible reduction of thermal conductivity [7,14,19]. A sensitivity study was conducted to investigate the effect of this simplification for selected cases (isolated pile and s = 2 m case). The specific heat capacity was selected as 1220 J/kg·°C, according to [34]. The thermal interface resistance (25 W/m^2·°C thermal conductance) between the concrete and soil was considered in the model [35]. Typical densities of the high-strength concrete (2450 kg/m^3) and sand (1600 kg/m^3) were used in the simulations.

In summary, a list of assumptions and simplifications used in the model is summarized as follows:

(1) A quarter symmetric 2D plane strain model was used.
(2) Symmetry boundary conditions were imposed with no heat flux transfer.
(3) The linear thermal material model was adopted in the main study.
(4) The concrete cracking effect was ignored.
(5) The change in the soil thermal conductivity over the moisture content was conservatively ignored.

4. Analytical Results and Discussions

4.1. Temperature Distribution in Concrete

This section discusses the effect of the group piles on temperature change and distribution inside the concrete section. Figure 6 illustrates the temperature distribution contours inside the concrete section at the end of several loading cycles for the s = 7 m case. Although the temperature at the inner surface comes back to 20 °C at the end of each cycle due to the imposed thermal loading cycle of the CAES (refer to Figure 4b), the heat penetrates the concrete section gradually and the temperature inside the concrete section increases with the cycles. The temperature is distributed uniformly along the circumferential direction because of symmetrical geometries and loading conditions. Therefore, the results in this section are presented and discussed along the radial direction at $\theta = 0°$

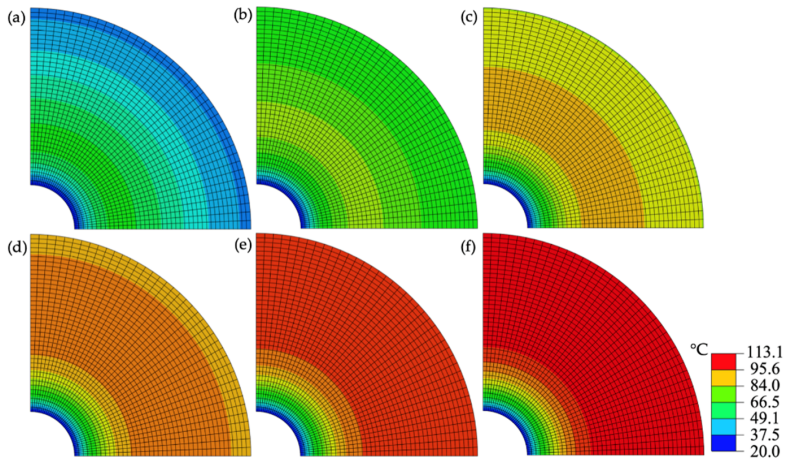

Figure 6. Temperature profile contour for concrete at the end of (**a**) the 1st loading cycle; (**b**) the 5th loading cycle; (**c**) the 50th loading cycle; (**d**) the 200th loading cycle; (**e**) the 400th loading cycle; and (**f**) the 1000th loading cycle.

Figure 7 represents the temperature history within several cycles for different pile spacing at (a) the one-third location ($r = \frac{2r_i+r_o}{3}$); (b) the two-thirds location ($r = \frac{r_i+2r_o}{3}$); and (c) the outer surface ($r = r_o$). Generally, the temperature change shows a cumulative effect and gradually increases with cycles. The increase in temperature is more rapid in early loading cycles than in the later ones. The group pile effect results in a temperature increase inside the concrete section due to the heat transferred from the adjacent piles. This effect was negligible in the earlier cycles since the heat from the adjacent pile was not reached yet. As the pile spacing becomes smaller, the effect of the adjacent pile starts to act earlier, resulting in a more rapid temperature increase. However, at the last loading cycle (1000), the temperatures in all group pile cases, regardless of the pile spacing, converge at a similar temperature, which is higher than the isolated pile case. In addition, comparing Figure 7a–c, it is noticeable that, moving away from the interior surface of the concrete section to the soil layer, the temperature fluctuation within each cycle becomes smaller.

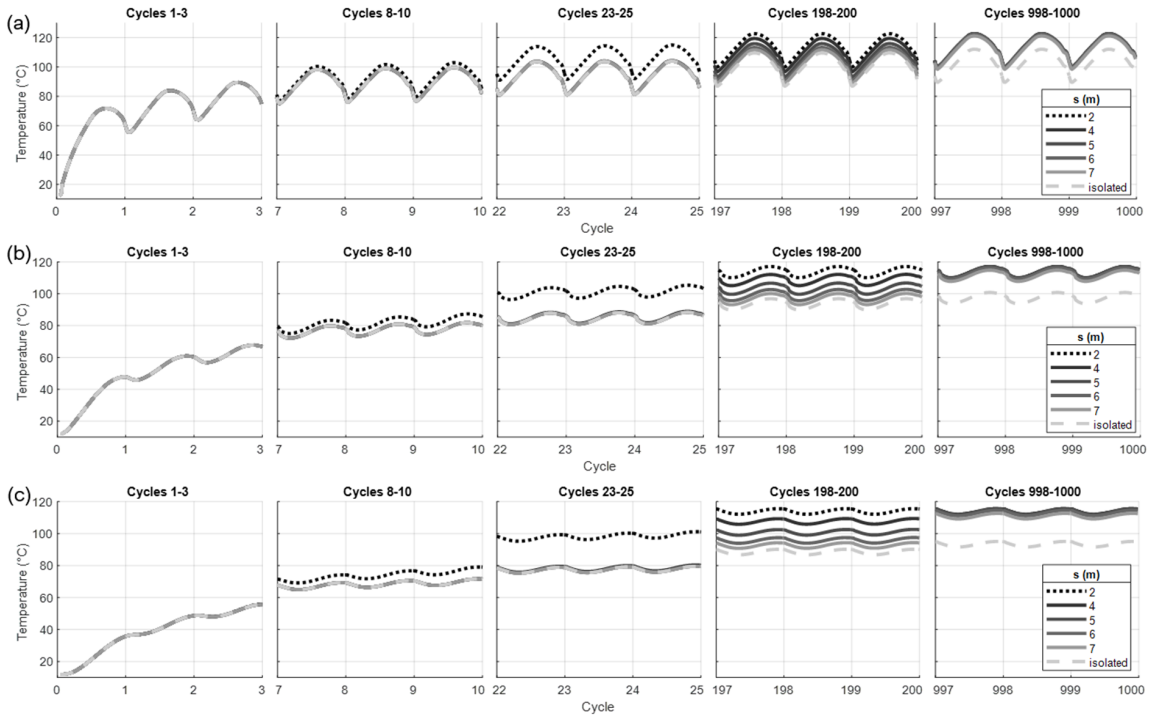

Figure 7. Temperature history within multiple loading cycles (1st–3rd, 8–10th, 23rd–25th, 198–200th, and 998–1000th) for different s at (**a**) the one-third location; (**b**) the two-thirds location; and (**c**) the outer surface.

Figure 8 shows the distribution of temperature along the concrete section for selected cycles at (a) the middle of a cycle (19:00) and (b) the end of a cycle (7:00). With the increase of loading cycles, the group pile effect tends to increase the temperature away from the inner surface. This trend results in a more uniform temperature distribution at 19:00 but a larger variation along the radial direction at 7:00. The group pile effect starts earlier for the cases with smaller pile spacing, but the temperature distribution in the last cycle converges to a similar distribution regardless of pile spacing.

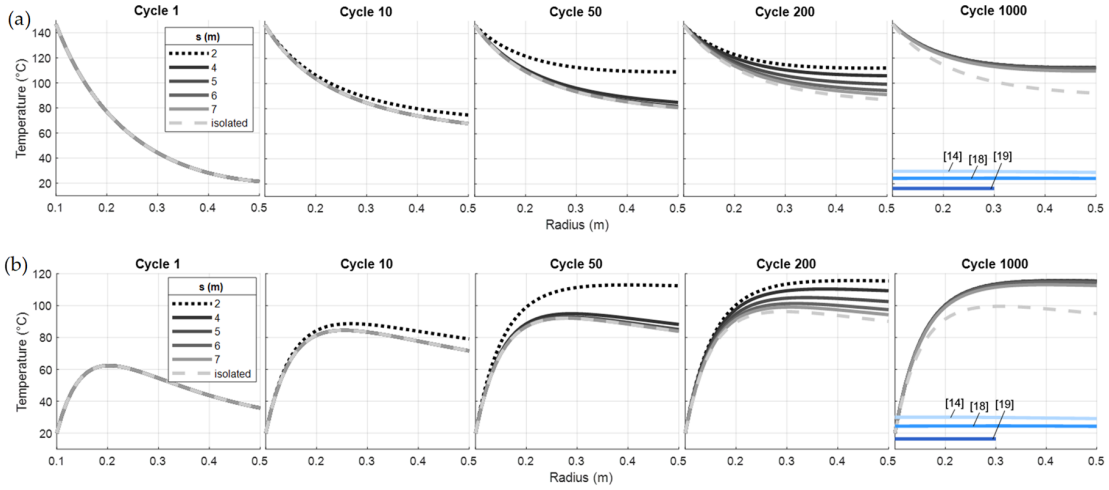

Figure 8. Distribution of the temperature along the radial direction in the 1st, 10th, 50th, 200th, and 1000th loading cycles at (**a**) 19:00 and (**b**) 7:00 (next day).

As a reference, the temperature distributions at steady state in the concrete section for the thermo-active pile from works of literature are shown as blue lines in Figure 8. As seen, the thermo-active pile shows a much lower temperature and a more uniform distribution as compared to the energy storage pile foundation due to differences in the thermal loading discussed in the Introduction section.

Figure 9 presents the highest temperature ever reached in each cycle for various pile spacing at (a) the one-third location ($\frac{2r_i+r_o}{3}$); (b) the middle location ($\frac{r_i+r_o}{2}$); (c) the two-thirds location ($\frac{r_i+2r_o}{3}$); and (d) the outer surface (r_o) of the concrete section. For all these cases, the maximum temperature increases as the loading cycle increases. As the cycle increases, the temperature change starts to slow down and converges at a constant temperature. The group pile cases converge to a significantly higher temperature (about 120 °C) than the isolated pile case due to the additional heat transferred from the adjacent piles. The cases with larger s have a lower converging speed compared to the cases with smaller pile spacing.

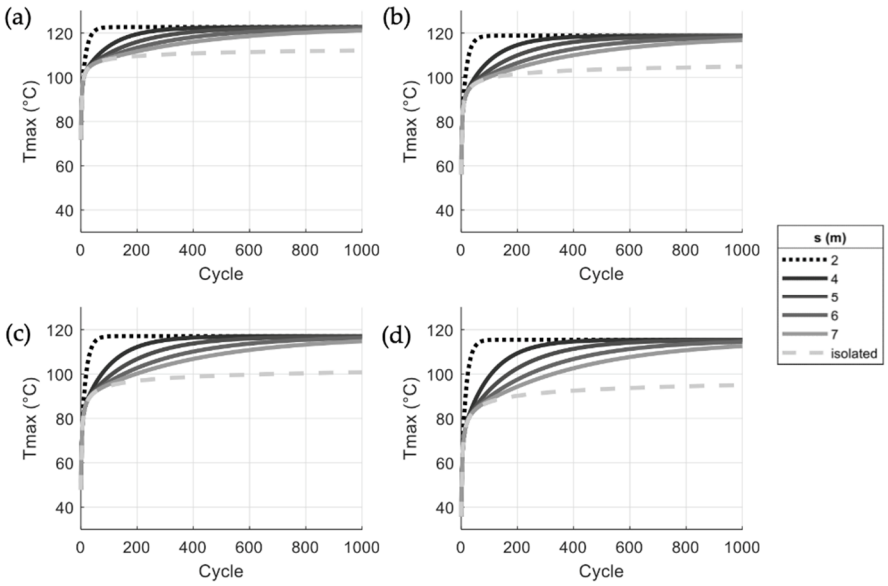

Figure 9. The largest temperature ever reached in each cycle for various s at (**a**) the one-third location; (**b**) the middle location; (**c**) the two-thirds location; and (**d**) the outer surface of the pile section.

To determine when the group pile starts to affect the temperature in the concrete section, a parameter N_G, which is calculated as the cycle where the maximum temperature difference (ΔT) between the group pile case and the isolated pile case starts to be higher than 0.1 °C at a given location of the pile section, was introduced. Figure 10a demonstrates an example with s = 2 m for the outer surface of the pile section on how N_G was determined, where at cycle 3, the maximum temperature difference starts to be larger than 0.1 °C.

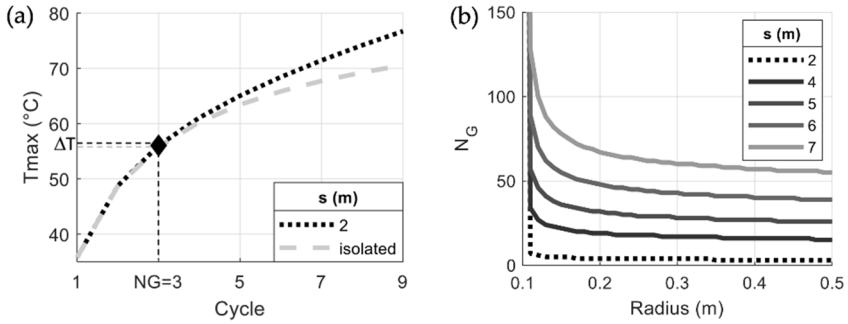

Figure 10. (**a**) Identification of cycles when group pile starts to affect the temperature (N_G) at the outer surface of the pile section; (**b**) N_G for each point of pile section.

Figure 10b shows N_G for all group pile cases along the concrete section. As seen from this figure, the inner surface of the concrete (r = 0.1 m) is not affected by the heat transferred from the adjacent pile, since the temperature at this surface follows the temperature input from compressed air and has the same profile for all cases, including the isolated pile. Moving further towards the outer surface of the concrete section, N_G gradually decreases, reaching a minimum value at the outer surface of the section (r = 0.5 m), which indicates that the heat from the adjacent pile affects the outer surface first, slowly transferring into the region closer to the inner surface. Regarding pile spacing, as the distance between two piles becomes gradually small, N_G also decreases.

4.2. Temperature Distribution in Soil

This section discusses the effect of group pile on temperature change and distribution inside the soil layer. Figure 11 demonstrates the temperature profile contours for surrounding soil at the end of selected loading cycles for the s = 7 m case. Similar to the concrete section, heat is gradually transferred into the soil from the pile, resulting in a gradual increase in temperature. As seen in Figure 11a–c, before the heat reaches the outer surface of the soil (center line between the two piles), the temperature inside the soil is distributed uniformly along the circumferential direction. As seen in Figure 11d–f, after the heat reaches the outer surface of the soil, the thermal effect of the adjacent pile starts and the temperature distribution along the circumferential direction is not uniform anymore. Therefore, this section will present and discuss temperature distribution along two radial directions: horizontal ($\theta = 0°$) and diagonal ($\theta = 45°$).

Figure 12 demonstrates the temperature history within several cycles for $\theta = 0°$ at (a) the inner surface of the soil (r_o); (b) the quarter of the soil layer ($\frac{s}{4} + \frac{r_o}{2}$); and (b) the center between two piles ($\frac{s}{2}$). In all cases, the temperature inside the soil gradually increases with the cycles, having a faster change at the earlier cycles. The group pile cases have a similar temperature at the location near the concrete pile in earlier cycles as the isolated pile case does. As the cycle increases, the group pile cases start to show a higher temperature than the isolated pile due to the heat transferred from the adjacent pile. The smaller the pile spacing and the further the location from the concrete section, the earlier this temperature difference starts. However, after a sufficient amount of cycles, the temperature in the soil tends to converge to a similar value (about 110 °C) for all group pile cases regardless of location. Such a phenomenon is different from the isolated pile case, where the temperature in the soil is stabilized at different values when moving away from the concrete pile.

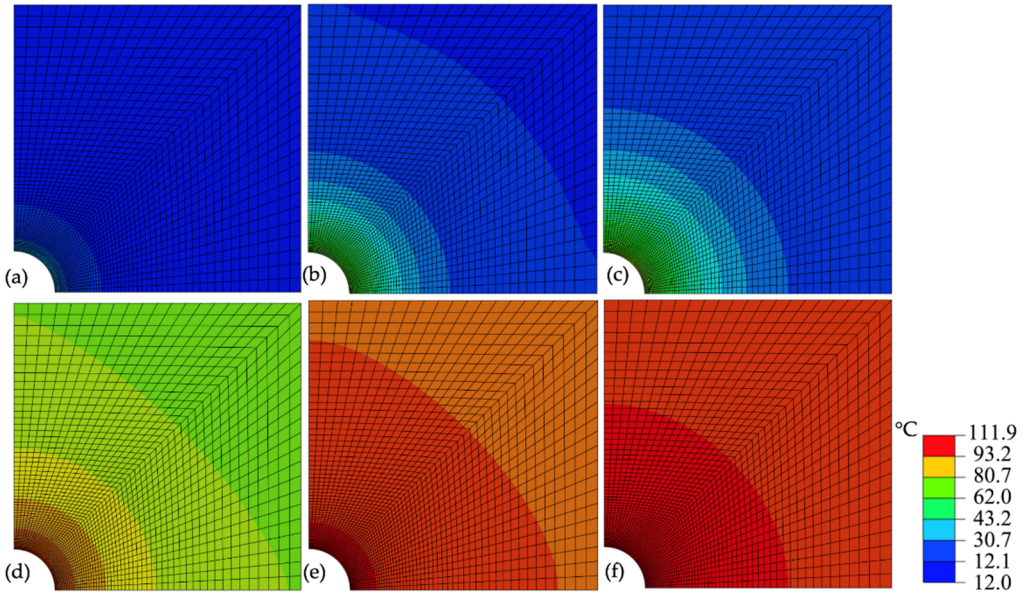

Figure 11. Temperature profile contour for soil at the end of (**a**) the 1st loading cycle; (**b**) the 13th loading cycle; (**c**) the 25th loading cycle; (**d**) the 400th loading cycle; (**e**) the 800th loading cycle; and (**f**) the 1000th loading cycle.

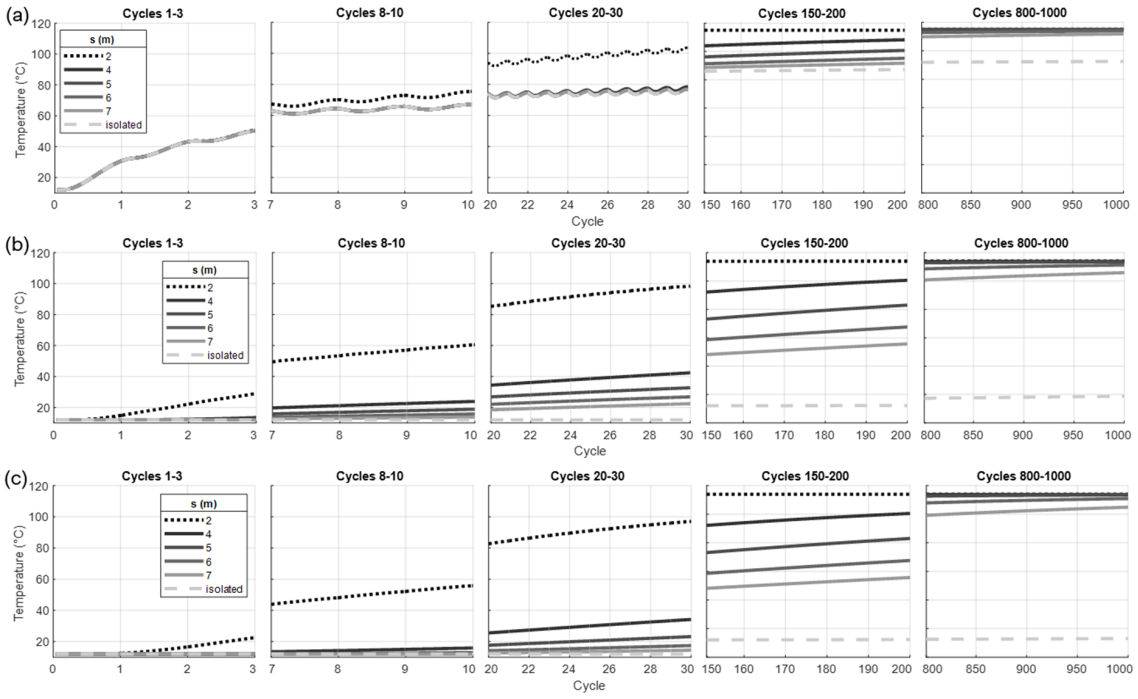

Figure 12. Temperature history within multiple cycles (1st–3rd, 8–10th, 20–30th, 150–200th, and 800–1000th) for θ = 0° at (**a**) the inner surface of the soil; (**b**) the quarter of the soil layer; (**c**) and the center between two piles.

Figure 13 shows temperature distribution along the radial direction in the soil at the end of each cycle for different pile spacings for (a) θ = 0° and (b) θ = 45°. As seen, temperature distribution along the radius follows the same trend for both the horizontal and diagonal directions. The group pile effect tends to make the temperature distribution more uniform in the soil with increase of the loading cycle. After a sufficient amount of cycles, the temperature distribution in all group pile cases reaches a similar constant pattern.

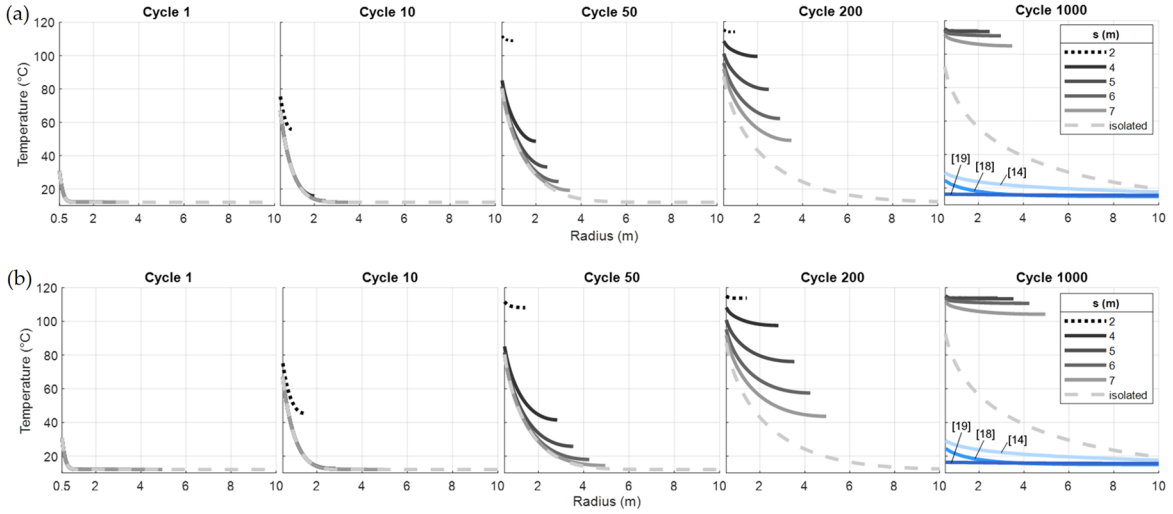

Figure 13. Temperature distribution along the soil section for different s at the end of the 1st, 10th, 50th, 200th, and 1000th loading cycles for (**a**) θ= 0° and (**b**) θ= 45°.

As a reference, the temperature distributions at steady-state in the soil for the thermo-active pile from works of literature are shown as blue lines in Figure 13. As seen, the thermo-active pile shows a much lower temperature as compared to the energy storage pile due to the differences in the thermal loading discussed in the Introduction section. The thermo-active pile and isolated energy storage pile show a similar temperature distribution trend: decreasing when moving away from the pile center, while the group energy storage pile shows a different uniform distribution due to the significant group pile effect.

Figure 14 illustrates the largest temperature ever reached within each cycle for various s at (a) the soil inner surface (r_o); (b) the quarter of the soil layer ($\frac{s}{4} + \frac{r_o}{2}$); and (c) the center between two piles ($\frac{s}{2}$) for both the horizontal (θ = 0°) and diagonal (θ = 45°) directions. As expected, the maximum temperature increases with the loading cycles but starts to slow down with increase of the cycles until it reaches a constant value. The cases with larger s show a slower convergence and converge at a similar but slightly lower temperatures compared to the cases with smaller s. In comparing the curves at different locations, it is seen that more cycles are required for temperature convergence when moving far from the pile. In addition, the cases with θ = 45° (Figure 14d–f) show similar convergence temperatures to those in the horizontal direction (Figure 14a–c).

Figure 15 shows N_G, calculated using the similar procedure demonstrated in Figure 10a, for each point of the soil layer for (a) θ = 0° and (b) θ = 45°. As expected, N_G decreases when moving far away from the concrete pile, which indicates that the locations near the center between two piles (r = s/2) first start to be influenced by the group pile effect. Then as the cycle increases, the heat from the adjacent pile starts to transfer into the soil layer further from the center line of adjacent piles, beginning to affect the temperature there. In addition, it is noted that the soil along the horizontal direction (Figure 15a) has lower N_G values than the soil along θ = 45° (Figure 15b), which means that the points at the horizontal line are affected first, since they are closer to the adjacent pile. As for pile spacing, piles located closer to each other show smaller N_G.

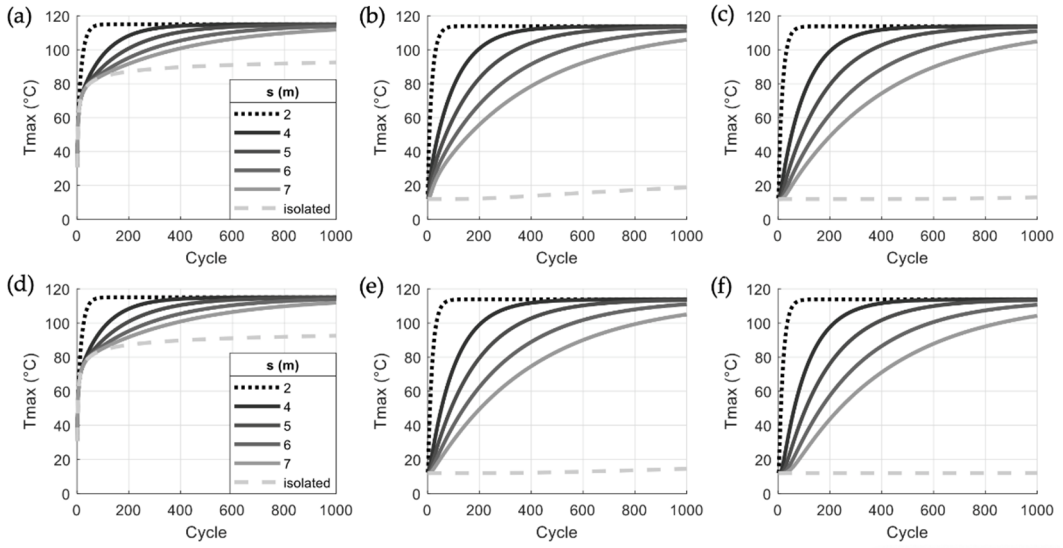

Figure 14. Maximum temperature in each loading cycle for different s at (**a**) the inner surface of the soil ($\theta = 0°$); (**b**) the quarter of the soil layer ($\theta = 0°$); (**c**) the center between two piles ($\theta = 0°$); (**d**) the inner surface of the soil ($\theta = 45°$); (**e**) the quarter of the soil layer ($\theta = 45°$); and (**f**) the center between two piles ($\theta = 45°$).

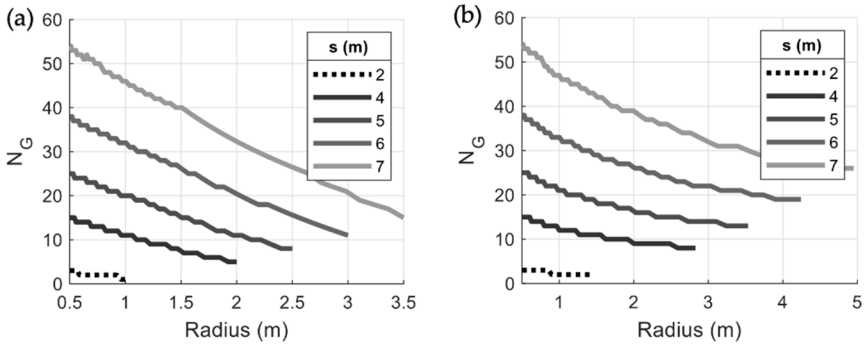

Figure 15. N_G for each point of the soil section for (**a**) $\theta = 0°$ and (**b**) $\theta = 45°$.

4.3. Sensitivity Study on the Thermal Property of the Soil

As discussed in Section 3.3, a simplified approach was used to model the thermal properties of the soil. This simplified model adopts a linear temperature independent of thermal conductivity for the soil. This simplification ignores the fact that the thermal conductivity of the soil will reduce due to moisture content reduction during cyclic heating of the pile. This section presents a sensitivity study on this simplification by directly comparing the results with a simplified linear thermal model to those with the nonlinear thermal model. The nonlinear thermal model adopts a temperature-dependent thermal conductivity for the soil. The thermal conductivity of the soil was assumed as 1.0 W/m·°C at the initial condition (12 °C) and then linearly reduces to 0.25 W/m·°C when the temperature increases to 100 °C following test results on the relationship of moisture content and thermal conductivity of the fine sand soil from [36].

Figure 16 shows the comparison of maximum temperature within each cycle for s = 2 m between the linear and nonlinear thermal models for (a) the concrete section and (b) the soil. Inside the soil, the nonlinear model shows a slightly slower convergence speed than the linear model but eventually converges to a similar temperature. This trend is due to the lower soil thermal conductivity used in the nonlinear model. For the concrete section, the nonlinear model has almost identical maximum temperature to the linear model. The temperature in the concrete section is heated from its own inner surface as well as adjacent piles. The lower soil thermal conductivity in the nonlinear thermal

model delays heat transfer from the concrete section to the soil. At the same time, it also delays temperature transfer from the adjacent pile to the concrete section. Thus, the combined action shows little temperature variation between the nonlinear and linear thermal model.

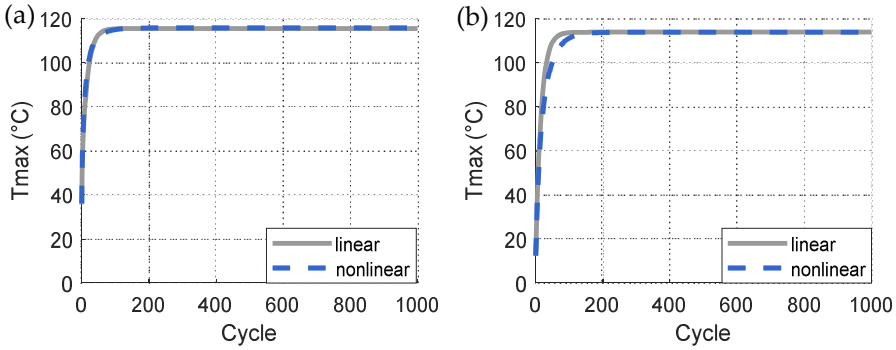

Figure 16. Comparison of maximum temperature with each cycle for s = 2 m between the linear and nonlinear thermal models: (**a**) the outer surface of the concrete section and (**b**) the center line between two piles.

Figure 17 shows the comparison of maximum temperature with each cycle in the concrete section for the isolated pile between the linear and nonlinear thermal models at (a) the midpoint and (b) the outer surface. As seen in Figure 17, the nonlinear thermal model shows higher temperature than the linear thermal model because the lower soil thermal conductivity helps the heat stay inside the concrete.

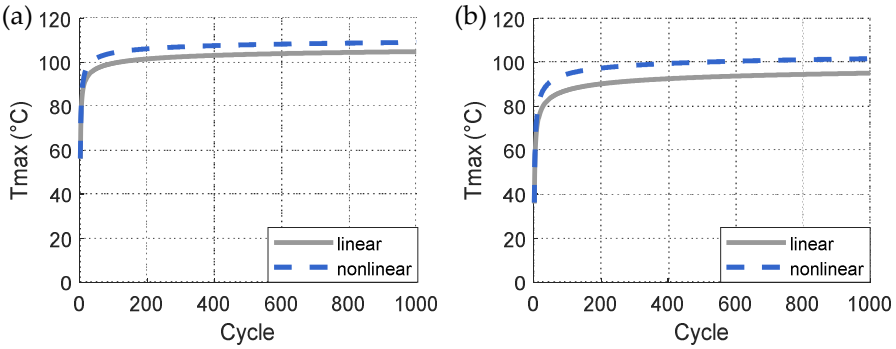

Figure 17. Comparison of maximum temperature with each cycle in the concrete section for the isolated pile between the linear and nonlinear thermal models at (**a**) the midpoint and (**b**) the outer surface of the pile section.

Figure 18 shows the comparison of temperature in the soil between the linear and nonlinear thermal models for the isolated pile cases: (a) maximum temperature at different locations and (b) temperature distribution along the radial direction at the end of 1000 cycle. The nonlinear thermal model predicts higher temperature near the concrete pile but shows a lower temperature far from the concrete pile since the lower thermal conductivity holds heat without transferring to a further distance. Eventually at a sufficiently far distance from the pile (r = 20.5 m), temperatures in both models are not affected and remain at the initial value.

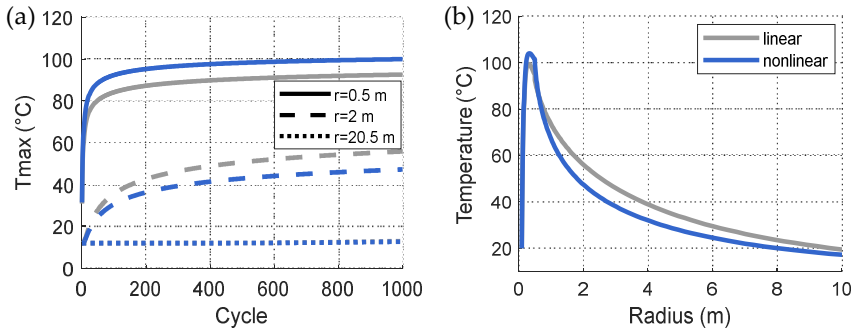

Figure 18. Comparison of temperature in the soil between the linear and nonlinear thermal models for the isolated pile cases: (**a**) maximum temperature at different locations and (**b**) temperature distribution along the radial direction at the end of 1000 cycle.

5. Conclusions

This paper studies the effect of group piles on temperature change and distribution inside the concrete pile and surrounding soil subjected to cyclic thermal loads. The thermal load is generated from the compressed air stored inside the pile. Two-dimensional symmetric models were developed for various pile spacing cases. The dynamic thermal transfer simulations were then carried out using these models. The following conclusions are drawn from the simulation results.

1. The group pile effect tends to increase the temperature up to more than 100 °C depending on the location inside both the soil and the concrete section due to the additional heat transferred from the adjacent pile. The amount of the increase becomes more significant when moving away from the center of the pile at a stabilized state.
2. As the increase of the loading cycles, the group pile effect firstly starts influencing the soil at the center line between two piles and then gradually affects other locations in the soil and concrete section when moving closer to the inner surface of the pile.
3. Temperature increase from the group pile effect is faster for the cases with smaller pile spacing in both the concrete section and the soil. However, the temperature tends to converge to a similar magnitude after enough cycles regardless of the spacing of the piles. The final stabilized temperature can be as high as 120 °C in the concrete pile and 110 °C in the soil after numerous loading cycles.
4. The group pile effect increases uniformity of the temperature distribution in the middle of the cycle but causes a less uniform distribution near the end of the cycle along the concrete section.
5. The group pile effect increases uniformity of the temperature distribution in the soil. After a sufficient amount of cycles, the distribution tends to become constant along the radial direction.
6. For the group pile case, the nonlinear thermal model with temperature-dependent soil thermal conductivity shows similar temperature distributions in both the concrete and the soil as that in the linear thermal model. For the isolated pile case, the nonlinear model predicts higher temperature in the concrete section and nearby soil layers but shows a lower temperature in the soil far from the concrete pile.
7. The temperature profiles obtained in this paper for different pile spacings are important for future thermal induced mechanical response studies. The temperature magnitude is about 4 times higher than that in typical thermal-active energy piles. The group pile effect is significant on the temperature distribution of the pile foundation and needs to be considered for the design of the energy storage pile foundation.

Author Contributions: Conceptualization, D.Z.; data curation, D.S. and Z.M.; formal analysis, D.S. and Z.M.; funding acquisition, D.Z., J.R.K., and D.L.; investigation, D.Z., Z.M., C.-S.S., and D.L.; methodology, D.Z., C.-S.S., and D.L.; project administration, J.R.K.; resources, C.-S.S., D.L., and J.R.K.; software, C.-S.S.; supervision, D.Z., C.-S.S., D.L., and J.R.K.; validation, D.S. and Z.M.; visualization, D.S. and Z.M.; writing—original draft, D.Z., Z.M., and D.S.; writing—review and editing, D.Z., C.-S.S., D.L., and J.R.K. All authors have read and agreed to the published version of the manuscript.

Funding: This research was supported by the Nazarbayev University Research Fund under grant #SOE2017001 and by the National Research Foundation of Korea (NRF) grant funded by the Korea government (MSIT) (2020R1F1A1048422).

Conflicts of Interest: The authors declare no conflict of interest.

References

1. Hayter, S.; Kandt, A. *Renewable Energy Applications for Existing Buildings (Technical Report NREL/CP-7A40-52172)*; National Renewable Energy Lab. (NREL): Golden, CO, USA, 2011. Available online: https://www.osti.gov/biblio/1022419 (accessed on 20 September 2020).
2. Rugolo, J.; Aziz, M. Electricity storage for intermittent renewable sources. *Energy Environ. Sci.* **2012**, *5*, 7151–7160. [CrossRef]
3. Sabirova, A.; Zhang, D.; Kim, J.; Nguyen, M.; Shon, C. Development of a reinforced concrete foundation system for renewable energy storage. In Proceedings of the 8th Asian Young Geotechnical Engineering Conference, Astana, Kazakhstan, 5–7 August 2016.
4. Tulebekova, S.; Saliyev, D.; Zhang, D.; Kim, J.; Karabay, A.; Turlybek, A.; Kazybayeva, L. Preliminary analytical study on the feasibility of using reinforced concrete pile foundations for renewable energy storage by compressed air energy storage technology. In *IOP Conference Series: Materials Science and Engineering*; IOP Publishing Ltd.: London, UK, 2017 November; pp. 12–23.
5. Tulebekova, S.; Zhang, D.; Lee, D.; Kim, J.; Barissov, T.; Tsoy, V. Nonlinear responses of energy storage pile foundations with fiber reinforced concrete. *Struct. Eng. Mech.* **2019**, *71*, 363–375.
6. Zhang, D.; Kim, J.; Tulebekova, S.; Saliyev, D.; Lee, D.H. Structural responses of reinforced concrete pile foundations subjected to pressures from compressed air for renewable energy storage. *Int. J. Concr. Struct. Mater.* **2018**, *12*, 74. [CrossRef]
7. Zhang, D.; Mamesh, Z.; Sailauova, D.; Shon, C.; Lee, D.H.; Kim, J. Temperature Distributions Inside Concrete Sections of Renewable Energy Storage Pile Foundations. *Appl. Sci.* **2019**, *9*, 4776. [CrossRef]
8. Laloui, L.; Nuth, M.; Vulliet, L. Experimental and numerical investigations of the behaviour of heat exchanger pile. *Int. J. Numer. Anal. Methods Geomech.* **2016**, *30*, 763–781. [CrossRef]
9. Bourne-Webb, P.; Amatya, B.; Soga, K. A framework for understanding energy pile behaviour. *Proc. Inst. Civ. Eng. Geotech. Eng.* **2013**, *166*, 170–177. [CrossRef]
10. Faizal, M.; Bouazza, A.; McCartney, J.S.; Haberfield, C. Effects of cyclic temperature variations on thermalresponse of an energy pile under a residential building. *J. Geotech. Geoenviron. Eng.* **2019**, *145*, 04019066. [CrossRef]
11. Murphy, K.D.; McCartney, J.S.; Henry, K.S. Evaluation of thermo-mechanical and thermal behavior offull-scale energy foundations. *Acta Geotech.* **2015**, *10*, 179–195. [CrossRef]
12. Di Donna, A.; Loria, A.F.R.; Laloui, L. Numerical study of the response of a group of energy piles underdifferent combinations of thermo-mechanical loads. *Comput. Geotech.* **2016**, *72*, 126–142. [CrossRef]
13. Surayatriyastuti, M.; Mroueh, H.; Burlon, S. Numerical analysis of a thermo-active pile under cyclic thermalloads. In Proceedings of the European Geothermal Conference (EGC 2013), Pisa, Italy, 3–7 June 2013; pp. 1–8.
14. Assunção, R.M. Thermal and Thermal-Mechanical Analysis of Thermo-Active Pile Foundations. Ph.D. Thesis, Instituto Superior Técnico, University of Lisbon, Lisbon, Portugal, 2014.
15. Tsetoulidis, C.; Naskos, A.; Georgiadis, K. Numerical investigation of the mechanical behaviour of single energy piles and energy pile groups. In Proceedings of the 1st International Conference on Energy Geotechnics, Kiel, Germany, 29–31 August 2016; pp. 569–575. [CrossRef]
16. Salciarini, D.; Ronchi, F.; Tamagnini, C. Thermo-hydro-mechanical response of a large piled raft equipped with energy piles: A parametric study. *Acta Geotech.* **2017**, *12*, 703–728. [CrossRef]
17. Mimouni, T.; Laloui, L. Behaviour of a group of energy piles. *Can. Geotech. J.* **2015**, *52*, 1913–1929. [CrossRef]
18. Ma, Q.; Wang, P. Underground solar energy storage via energy piles. *Appl. Energy* **2020**, *261*, 114361. [CrossRef]

19. Olgun, C.G.; Ozudogru, T.Y.; Abdelaziz, S.L.; Senol, A. Long-term performance of heat exchanger piles. *Acta Geotech.* **2015**, *10*, 553–569. [CrossRef]
20. Energy Storage Association, Compressed Air Energy Storage. 2020. Available online: http://energystorage.org/compressed-air-energy-storage-caes (accessed on 12 August 2020).
21. Kodur, V. Properties of concrete at elevated temperatures. *ISRN Civ. Eng.* **2014**, 1–15. [CrossRef]
22. Choi, Y.S.; Lee, J.; Prezzi, M.; Salgado, R. Response of pile groups driven in sand subjected to combined loads. *Geotech. Geol. Eng.* **2017**, *35*, 1587–1604. [CrossRef]
23. Noman, B.J.; Abd-Awn, S.H.; Abbas, H.O. Effect of Pile Spacing on Group Efficiency in Gypseous Soil. *Civ. Eng. J.* **2019**, *5*, 373–389. [CrossRef]
24. Souri, A.; Abu-Farsakh, M.Y.; Voyiadjis, G.Z. Evaluating the effect of pile spacing and configuration on the lateral resistance of pile groups. *Mar. Georesour. Geotech.* **2020**, 1–13. [CrossRef]
25. Murthy, V.N.S. *Advanced Foundations Engineering-Geotechnical Engineering Series*; CBS Publisher & Distributors: New Delhi, India, 2010; pp. 251–534.
26. Das, B. *Principles of Foundation Engineering*, 9th ed.; Cengage Learning: Stamford, CT, USA, 2011; pp. 617–619.
27. Zhang, D.; Fleischman, R.B. Establishment of performance-based seismic design factors for precast concrete floor diaphragms. *Earthq. Eng. Struct. Dyn.* **2006**, *45*, 675–698. [CrossRef]
28. Simulia Abaqus, "Abaqus CAE Theory Guide". Available online: http://130.149.89.49:2080/v2016/books/stm/default.htm?startat=ch02s04ath19.html (accessed on 12 August 2020).
29. Bektimirova, U.; Shon, C.; Zhang, D.; Sharafutdinov, E.; Kim, J. Proportioning and characterization of reactive powder concrete for an energy storage pile application. *Appl. Sci. Switz.* **2018**, *8*, 2507. [CrossRef]
30. Brandl, H. Energy foundations and other thermo active ground structures. *Geotechnique* **2016**, *56*, 81–122. [CrossRef]
31. Kodur, V.; Khaliq, W. Effect of temperature on thermal properties of different types of high-strength concrete. *J. Mater. Civ. Eng.* **2011**, *23*, 793–8011. [CrossRef]
32. Shon, C.S.; Mukashev, T.; Lee, D.H.; Zhang, D.; Kim, J.R. Can Common Reed Become an Effective Construction Material? Physical, Mechanical, and Thermal Properties of Mortar Mixture Containing Common Reed Fiber. *Sustainability* **2019**, *11*, 903. [CrossRef]
33. Lee, S.J.; Kim, K.Y.; Choi, J.C.; Kwon, T.H. Experimental investigation on the variation of thermal conductivity of soils with effective stress, porosity, and water saturation. *Geomech. Eng.* **2016**, *11*, 771–785. [CrossRef]
34. Yoon, S.; Lee, S.R.; Go, G.H.; Jianfeng, X.; Park, H.; Park, D. Thermal transfer behavior in two types of W-shape ground heat exchangers installed in multilayer soils. *Geomech. Eng.* **2014**, *6*, 79–98. [CrossRef]
35. Thomas, H.R.; Rees, S.W. Measured and simulated heat transfer to foundation soils. *Géotechnique* **2009**, *59*, 365–375. [CrossRef]
36. Haigh, S.K. Thermal conductivity of sands. *Geotechnique* **2012**, *62*, 617–625. [CrossRef]